Table 2 PCM property values[a]

Materials	Transition temperature,[1] K	Transition enthalpy,[2] KJ/Kg	Specific heat,[3] KJ/Kg-K
Solid-solid			
NPG	321	119	2.7
PG	355	139	2.8
Solid-liquid			
MCH	390	169	2.3
SSD	304	186	3.1
Mixtures (molar ratio)			
NPG-MCH (7:3)	316	87	1.5
NPG-MCH (9:1)	315	101	2.1
NPG-SSD (7:3)	362	56	0.2
NPG-SSD (9:1)	313	108	1.4
PG-MCH (7:3)	358	56	1.0
PG-MCH (9:1)	358	67	—
PG-SSD (7:3)	343	260	0.7
PG-SSD (9:1)	360	241	2.0

[a]Measurement uncertainty of 1) ±1 K; 2) ±1 KJ/Kg; 3) ±10%.

Phase-Change Property Determinations

A Perkin-Elmer differential scanning calorimeter DCS-2 was used to measure the transition temperature, enthalpies of transformation, and heat capacities of the subject phase-change materials. Thermal analysis samples consisted of carefully weighed portions of the finely powdered compounds. Mixtures were prepared by grinding together gram-size portions of the components and then extracting milligram-size samples for analysis. Table 2 shows the results of DSC measurements for phase-change characteristics of neopentyl glycol and pentaglycerine with mixing of additives.

Mixing neopentyl glycol with magnesium chloride hexahydrate lowers both enthalpy of transformation and specific heat; again, incongruent melting behavior of magnesium chloride hexahydrate deteriorates the solid-state transformation, even though transformation occurs near the neopentyl glycol phase-change transition temperature. The mix of neopentyl glycol with sodium sulfate decahydrate also lowers both the enthalpy of transformation and the specific heat by almost the same magnitude as did the mix of magnesium chloride hexahydrate. For a molar ratio of 7:3, results were largely unpredictable due to the incongruent melting behavior of the neopentyl glycol mix with sodium sulfate decahydrate. Also, the phase transformation was barely discernible with this mixture and occurred at a higher temperature.

Mixtures of pentaglycerine with magnesium chloride hexahydrate or sodium sulfate decahydrate also did not prove attractive. Similar incongruent melting behavior was observed, as with the neopentyl glycol; the phase transformation temperature was almost unchanged. Thus, the pentaglycerine mixes' phase-change occurs higher than the desired battery operation temperature range.

Sublimation Test Results

Sublimation tests on neopentyl glycol were conducted at NASA Johnson Space Center in a vacuum chamber. Sublimation of neopentyl glycol is a very serious problem at vacuum conditions (pressure $<10^{-6}$ torr). As the temperature of neopentyl glycol at vacuum conditions increased, the sublimation rate linearly increased from 300 mg/hr/g at 25°C to 800 mg/hr/g at 55°C. Several ways of eliminating this sublimation at vacuum conditions were tried, including enamel based paint and microencapsulation of the neopentyl glycol, but the coating was too porous to sustain the sublimation pressure. Macroencapsulation, using containment of the entire storage material, seems to be the most feasible approach to controlling sublimation.

Conclusion

An investigation into using solid-solid phase-change materials in space-suit battery packs for temperature control led to the aluminum foam/neopentyl glycol combination as the premiere candidate. The combination of high thermal conductivity and latent heat appears to be appropriate for maintaining battery operation at fairly low temperatures over extended time periods. The problem of neopentyl glycol sublimation at vacuum conditions appears to be best approached by sealing the entire storage material.

References

[1]*Manned Space Vehicle Battery Safety Handbook,* NASA Johnson Space Center Rept. JSC-20793, Sept. 1985.

[2]Lane, G. A., *Solar Heat Storage: Latent Heat Storage,* Vol. 1, CRC Press, Boca Raton, FL, 1988.

[3]Benson, D. K., Burrows, R. W., and Webb, J. D., "Solid State Phase Change Transitions in Pentaerythritol and Related Polyhydric Alcohols," *Solar Energy Materials,* Vol. 13, 1986, pp. 133–152.

[4]Hooper, F. C., and Lepper, F. R., "Transient Heat Flow Apparatus for the Determination of Thermal Conductivities," *Transactions of The American Society of Heating and Ventilating Engineers,* Vol. 56, No. 1395, 1950, pp. 309–324.

[5]"Eastman NPG Glycol as a Thermal Storage Medium," EPC 4909, Eastman Chemical Products, Kingsport, TN.

[6]Taylor, R. E., and Groot, H., "Thermal Conductivity of Eastman NPG Glycol," Rept. to Tennessee Eastman Co., Purdue Univ., West Lafayette, IN, TPRL 480, 1985.

[7]Siegel, R., "Solidification of Low Conductivity Material Containing Dispersed High Conductivity Particles," *International Journal of Heat and Mass Transfer,* Vol. 20, No. 10, 1977, pp. 1087–1089.

Large Eddy Simulation of the Flow in a Transpired Channel

Ugo Piomelli*
University of Maryland,
College Park, Maryland 20742
and
Parviz Moin† and Joel Ferziger‡
Stanford University, Stanford, California 94305

Introduction

TRANSPIRATION (or blowing) is often used to protect the surface of a material exposed to a hot freestream: cool fluid is injected through the surface, which must be porous. Suction is used to delay boundary-layer separation in aeronautical applications. Between 1967 and 1975, many experiments were caried out on the characteristics of transpiration on boundary layers.[1-3] The effect of transpiration on the velocity field in the boundary layer was found to be significant: when fluid is injected ("blowing"), the boundary layer becomes thicker, the skin friction decreases, and turbulent fluctuations are enhanced. If suction is applied, the effect is the opposite in each instance. Turbulent boundary layers with transpiration

Received Feb. 6, 1989; revision received and accepted for publication Oct. 24, 1989.

*Assistant Professor, Department of Mechanical Engineering. Member AIAA.

†Associate Professor, Department of Mechanical Engineering; also with NASA Ames Research Center, Moffett Field, California. Member AIAA.

‡Professor, Department of Mechnical Engineering. Member AIAA.

were chosen as test cases by the Air Force Office of Scientific Research/Heat Transfer and Turbulence Mechanics-Stanford Conference on Complex Turbulent Flows.[4] A variety of turbulence models (one- and two-equation, as well as Reynolds stress models) were used to predict turbulent statistics for various transpiration rates and pressure gradients. Although the mean velocity profiles predicted by the models were in reasonable agreement with the experimental data, streamwise development of skin-friction coefficients and momentum and displacement thickness were not predicted accurately, especially in the presence of suction.

In the present study, we apply the large eddy simulation (LES) technique to compute the flow in a fully developed transpired channel. In LES, the dynamics of the large energy-carrying structures are computed accurately, so that detailed information on turbulent structures is available for the development of more accurate turbulence and wall layer models. Moin[5] reported the skin-friction coefficient obtained from a large eddy simulation of turbulent channel flow with transpiration, which was found to agree well with the experimental results for transpired boundary layers. Moin, however, did not show any statistical quantity other than the skin-friction coefficient. Although no experimental study of this flow has been made, the physical phenomena encountered in a transpired channel are sufficiently similar to those in a boundary layer to allow comparison with the boundary-layer results. Fully developed transpired channel flow, moreover, provides an ideal test case for turbulence models, since the flow is one-dimensional in the mean (function of y only) and only wall boundary conditions are required. The turbulent transport equations become ordinary differential equations.

Numerical Method

In LES, we decompose the flow variables (velocity u_i and pressure p) into a large-scale component (denoted by an overbar) and a subgrid component (denoted by a prime). A large scale quantity is defined by the filtering operation:

$$\bar{f}(x) = \int_D G(x,x')f(x')\,dx' \tag{1}$$

where the integral extends over the entire domain D, and G is the filter function. In the present work, the Gaussian filter is used in the streamwise and spanwise directions; a sectionally continuous top-hat filter is applied in the normal direction.[6]

The filtered Navier-Stokes and continuity equations, which describe the evolution of the large energy-carrying eddies, can be obtained by applying the filtering operation to the Navier-Stokes and continuity equations to yield

$$\frac{\partial \bar{u}_i}{\partial t} + \frac{\partial}{\partial x_j}\left(\overline{\bar{u}_i\bar{u}_j}\right) = -\frac{\partial \bar{p}}{\partial x_i} - \frac{\partial \tau_{ij}}{\partial x_j} + \frac{1}{Re_\tau}\frac{\partial^2 \bar{u}_i}{\partial x_j \partial x_j} \tag{2}$$

$$\frac{\partial \bar{u}_i}{\partial x_i} = 0 \tag{3}$$

in which all quantities are made dimensionless by the channel half-width δ and the wall shear velocity $u_\tau^{av} = (\tau_w^{av}/\rho)^{1/2}$, where τ_w^{av} is the average wall stress on the two sides of the channel and ρ is the fluid density. The effect of the subgrid scales appears in the residual stress

$$\tau_{ij} = \overline{u_i u_j} - \overline{\bar{u}_i \bar{u}_j} \tag{4}$$

which, in the present study, was parameterized by the mixed model[6,7]

$$\tau_{ij} = \bar{u}_i\bar{u}_j - \overline{\bar{u}_i\bar{u}_j} - 2\nu_T S_{ij} \tag{5}$$

in which S_{ij} is the large-scale strain-rate tensor

$$S_{ij} = \frac{1}{2}\left(\frac{\partial \bar{u}_i}{\partial x_j} + \frac{\partial \bar{u}_j}{\partial x_i}\right) \tag{6}$$

and ν_T is an eddy diffusivity given by[8]

$$\nu_T = l^2\sqrt{2S_{ij}S_{ij}} \tag{7}$$

in which l is a length scale representative of the small eddies and is related to the grid size.

No-slip conditions were applied at the walls, and periodic boundary conditions were imposed at the streamwise and spanwise boundaries. The numerical method used to integrate Eqs. (3) and (4) is based on the work of Moin et al.[9] Fourier expansions are employed in the streamwise and spanwise directions, and finite differences are used in the normal direction; aliasing errors are eliminated using the 3/2 rule.

Results and Discussion

In fully developed channel flow with transpiration, fluid is injected uniformly through the lower wall ($y = -1$) and removed at the same rate through the upper one ($y = 1$). Two transpiration rates were used in this study: $v_o = 0.09$ and $v_o = 0.04$. The first is a rather high transpiration rate. The blowing fractions $F = v_o/U_{max}$ in the two cases, and the transpiration rates normalized by the local shear velocities (the superscripts b and s denote, respectively, the blowing and suction sides of the channel) u_τ^b and u_τ^s are reported in Tables 1 and 2. The Reynolds number Re_θ is based on the momentum thickness θ and the maximum mean velocity, $b_f = 2F/c_{f,NT}$ is a dimensionless blowing parameter, and $c_{f,NT}$ is the skin-friction coefficient in the absence of transpiration. The skin-friction coefficient was calculated according to the definition

$$c_f = \frac{\tau_w}{\rho U_{\max}^2/2} \tag{8}$$

The length of the computational domain was $L_x = 3\pi\delta$ in the streamwise direction x, $L_z = \pi\delta$ in the spanwise direction z; 32 grid points were employed in x and z, and 63 points in the normal direction y. The mesh was uniform in the streamwise and spanwise directions and clustered near the wall in the normal direction, using exponential stretching.

The mean velocity profiles normalized by the local wall shear velocity are shown in Fig. 1 (a superscript + indicates

Table 1 Summary of results, strong transpiration

	Blowing		Suction	
	LES	Experiment[a]	LES	Experiment[b]
	0.0516	0.0517	−0.034	−0.035
$F\times10^3$	4.00	3.75	−4.00	−4.00
Re_θ	1670	3030	1670	272
v_o^+	0.154	0.147	−0.060	−0.059
$c_f/c_{f,NT}$	0.340	0.343	2.263	2.214
b_f	2.030	2.071	−2.030	−1.912

[a]Andersen et al.[3] [b]Julien et al.[2]

Table 2 Summary of results, weak transpiration

	Blowing		Suction	
	LES	Experiment[a]	LES	Experiment[b]
$F\times10^3$	1.88	2.00	−1.88	−2.00
Re_θ	1195	1034	1195	427
v_o^+	0.0516	0.0517	−0.034	−0.035
$c_f/c_{f,NT}$	0.602	0.680	1.352	1.480
b_f	0.85	0.90	−0.85	−0.91

[a]Andersen et al.[3] [b]Julien et al.[2]

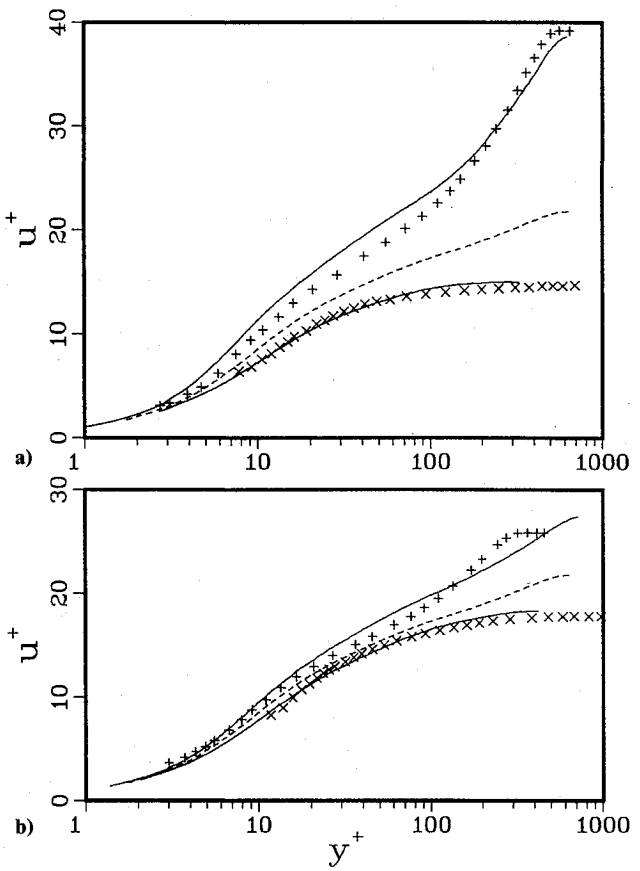

Fig. 1 Mean velocity profile in wall coordinates: —— transpiration; ---- no transpiration; + Andersen et al.[3] (blowing); × Julien et al.[2] (suction); a) strong transpiration, b) weak transpiration.

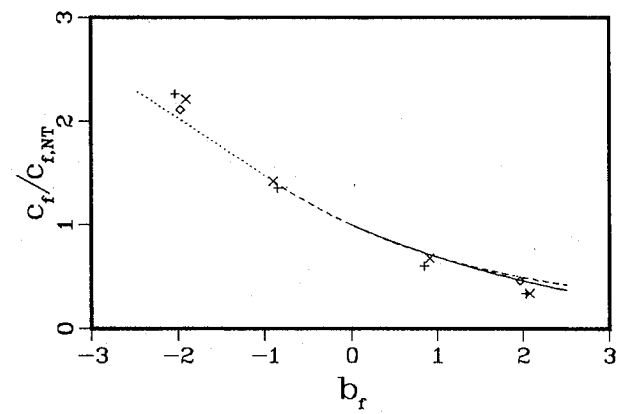

Fig. 2 Ratio of friction coefficient to friction coefficient without transpiration: + present calculation; ◇ Moin[5]; × experiments, Andersen et al.[3] (blowing), and Julien et al.[2] (suction); —— correlation of experimental results, Andersen et al.[3]; ---- correlation of experimental results, Simpson et al.[1]; ····· extrapolation of Simpson et al.[1] correlation.

quantities made dimensionless by the local shear velocities, u_τ^b or u_τ^s, and the kinematic viscosity ν). They agree well with the experimental results. The differences are due, at least in part, to the different blowing rates and Reynolds numbers between the simulation and experiments. The fact that better agreement with the experimental results is found for the strong transpiration case may also be because the transpiration rates match more closely in that case.

The skin-friction coefficient obtained from the simulation agrees well with the experimental data[1,3] (Fig. 2). The rms intensities of the fluctuating velocity components $u_i'' = u_i - U_i$ (in which U_i is the long-time mean of u_i) normalized by u_τ^{av}

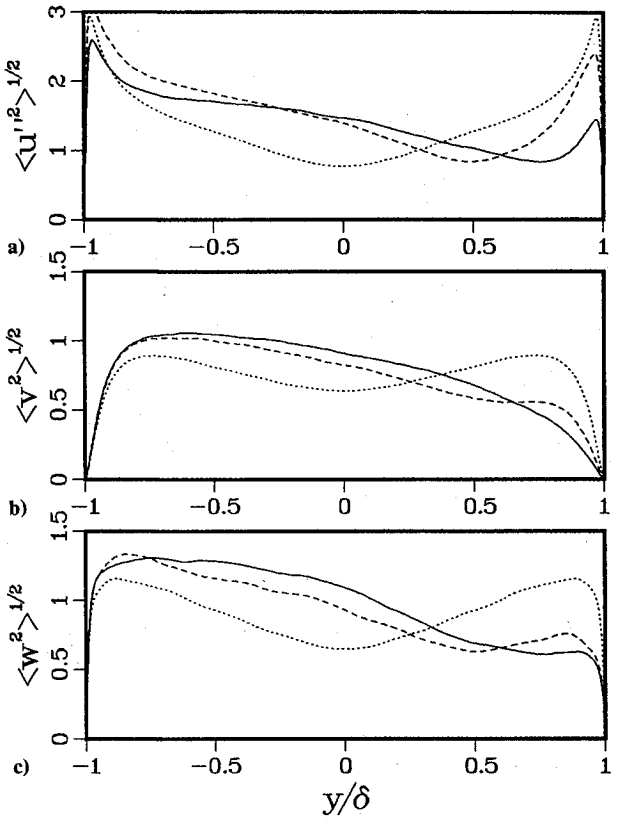

Fig. 3 Turbulence intensities: —— strong transpiration; ---- weak transpiration; ····· no transpiration; a) u'', b) v, c) w.

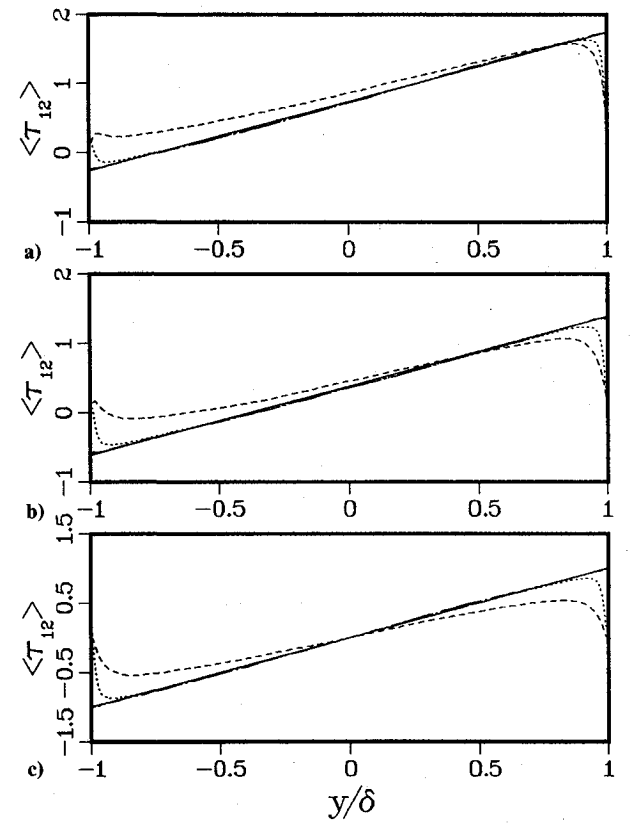

Fig. 4 Shear stress profile: ---- resolved; ····· resolved + SGS; —·— total; a) strong transpiration, b) weak transpiration, c) no transpiration.

(Fig. 3) are significantly reduced on the suction side. In local coordinates, the maximum streamwise rms intensity occurs at $y^+ = 12$ on the blowing side and $y^+ = 36$ on the suction side for the strong transpiration rate, and at $y^+ = 16$ on the blow-

ing side and $y^+ = 24$ on the suction side for weak transpiration. In the absence of transpiration, the maximum streamwise turbulence intensity occurs at $y^+ = 16$. If the location of maximum streamwise turbulence intensity is used as a measure of the wall layer thickness, the effect of transpiration is to make the wall layer thinner, in local coordinates, in the case of blowing, and thicker in the case of suction; however, the physical (unnormalized) thickness increases slightly on the blowing side and decreases on the suction side. The shear stress profiles (Fig. 4) show increased stress on the suction side and decreased stress on the blowing side. Transpiration shifts the point where $\langle -u''v'' \rangle = 0$ (where $\langle \cdot \rangle$ indicates time-averaging) toward the blowing wall, whereas the location where $dU/dy = 0$ is moved toward the suction wall. These effects cannot be predicted simultaneously by eddy viscosity models, which require that $\langle -u''v'' \rangle$ and dU/dy be zero at the same point.

Although blowing was not found to affect the spectra very much, when suction is applied, turbulence structures with small streamwise wavelength appeared to be significantly attenuated. As a result, streamwise velocity fluctuations are more strongly correlated in the presence of suction (Fig. 5a), and the streak spacing λ^+ is increased (Fig. 5b). Although the spanwise resolution of the present simulation ($\Delta z^+ \simeq 62$ for the nontranspired case) results in an excessive mean streak spacing for all cases examined, the qualitative increase in λ^+ due to suction may be realistic. When the channel half-width is used to normalize the separation (Fig. 6), the differences between the two-point correlations are smaller. Generally, use of global coordinates (average wall stress, channel half-width) led to improved collapse of the statistics.

To investigate the effect of transpiration on the inclination of the wall layer structures, the two-point correlation coefficient $R_{u\tau}$ between $\tau_{12,w}(x'+x,z')$ and $u(x',y,z')$ was computed as a function of the streamwise separation (normalized by the computational box length L_x) for different values of $y_w = 1 - |y|$ (Fig. 7). For the nontranspired channel, the results are similar to those obtained experimentally by Rajagopalan and Antonia.[10] The maximum correlation coefficient is approximately 0.6 and is achieved with the velocity measured downstream of the wall stress. The displacement of the correlation peak indicates that the structures responsible for this correlation lie at an angle of about 8 deg, with the wall at $y^+ = 35$, a value consistent with the experimental results.[10] On

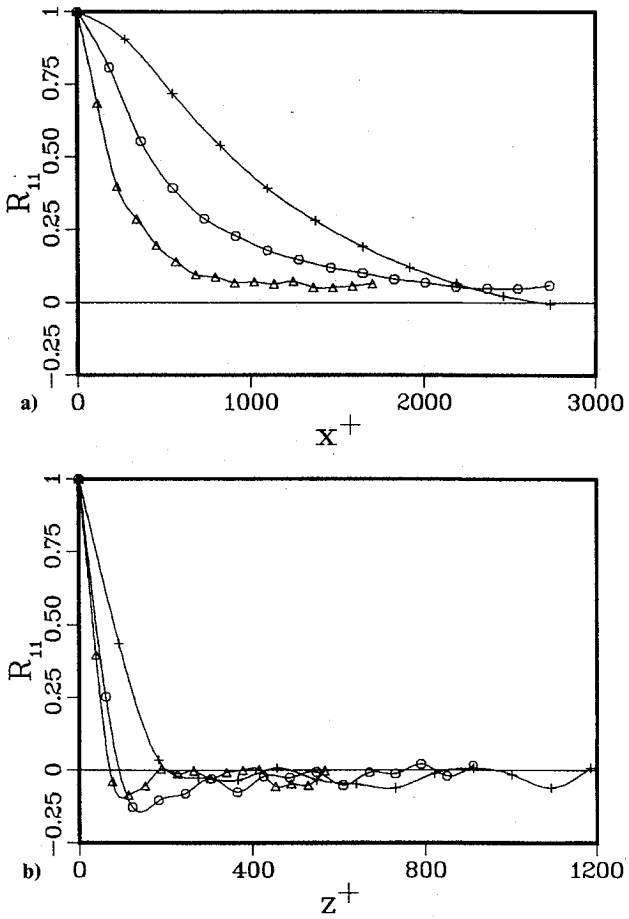

Fig. 5 Two-point correlation coefficient R_{11} in local coordinates at the location of maximum streamwise turbulence intensity: o, no transpiration; Δ, strong blowing; +, strong suction; a) streamwise separation, b) spanwise separation.

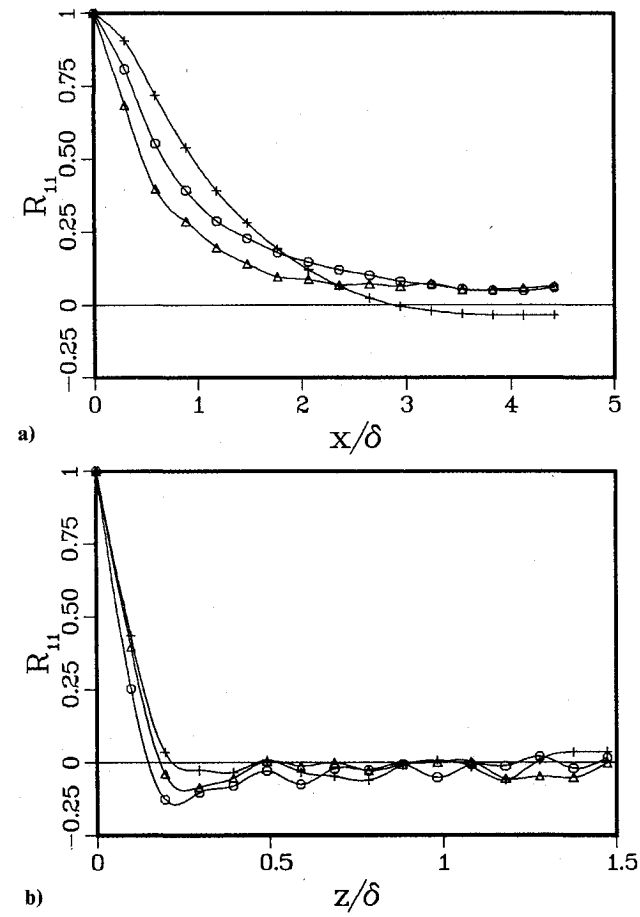

Fig. 6 Two-point correlation coefficient R_{11} in global coordinates at the location of maximum streamwise turbulence intensity: o, no transpiration; Δ, strong blowing; +, strong suction; a) streamwise separation, b) spanwise separation.

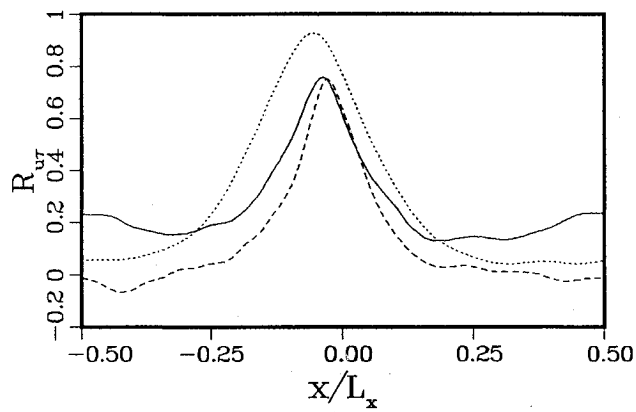

Fig. 7 Correlation coefficient between $\tau_{12,w}$ and u at $y_w = 0.049$: —— no transpiration; ---- strong transpiration, blowing side; ····· strong transpiration, suction side.

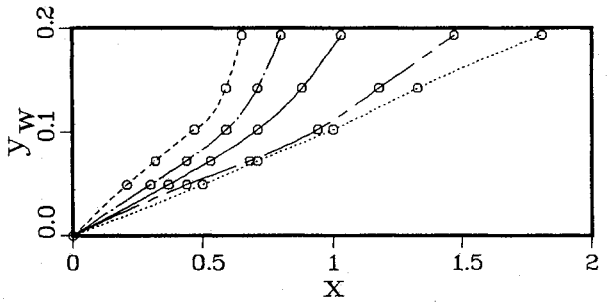

Fig. 8 Locus of the peak of the correlation between $\tau_{12,w}$ and u: —— no transpiration; ---- strong transpiration, blowing side; ····· strong transpiration, suction side; —·— weak transpiration, blowing side; —— weak transpiration, suction side.

the blowing side of the channel, the correlation coefficient $R_{u\tau}$ is similar to that in the nontranspired channel, but the displacement of the correlation peak is significantly smaller, whereas on the suction side, the shift of the correlation peak is larger than in the nontranspired channel and the correlation coefficient is higher. The locus of maximum correlation is illustrated in Fig. 8 for all of the cases examined. The curves in Fig. 8 represent the shape of the structures responsible for the correlation between velocity and stress; the effect of transpiration is to increase the inclination of the near-wall structures with respect to the wall when blowing is applied and to decrease it when suction is applied.

Conclusions

The flow in a transpired channel has been computed by large eddy simulation. Mean velocity profiles and skin-friction coefficients compare well with experimental data. Blowing decreases the shear stress and enhances turbulent fluctuations, whereas suction has the opposite effect. Although in this flow strong nongradient effects are present that make eddy viscosity turbulence models inapplicable, LES successfully predicts velocity and Reynolds stress profiles that display a shift between the locations in which the Reynolds stress and the mean velocity gradient are zero. The wall layer thickness normalized by the local shear velocity and kinematic viscosity decreases on the blowing side of the channel and increases on the suction side. The unnormalized wall layer thickness, however, has opposite behavior, increasing on the blowing side and decreasing on the suction side. The displacement of the point of maximum velocity toward the suction wall appeared to be the principal effect of transpiration.

The two-point correlations indicate that suction decreases the energy content of the small scales of turbulence and increases the mean streak spacing (in wall units). Blowing has the opposite effect on the mean streak spacing. The mean streak spacing in global coordinates is affected by transpiration to a much smaller extent, indicating that the change in λ^+ may be due mostly to the change in the wall stress. The resolution of the present calculations was, however, insufficient to allow conclusive statements to be drawn regarding the effect of transpiration on the streak spacing. More finely resolved simulations are required to determine whether transpiration has any effect on the physical streak spacing. The correlation between velocity and wall stress was also computed. On the blowing side, the wall layer structures lie at a steeper angle to the wall, whereas on the suction side this angle is shallower.

Acknowledgments

This work was supported by NASA under Cooperative Agreement NCC 2-15. The authors thank John Kim of NASA Ames Research Center for many valuable discussions.

References

[1]Simpson, R.L., Moffat, R.J., and Kays, W.M., "The Turbulent Boundary Layer on a Porous Plate: Experimental Skin Friction with Variable Injection and Suction," *International Journal of Heat and Mass Transfer,* Vol. 12, 1969, pp. 771–789.

[2]Julien, H.L., Kays, W.M., and Moffat, R.J., "Experimental Hydrodynamics of the Accelerated Turbulent Boundary Layer with and without Mass Injection," *ASME Journal of Heat Transfer,* Vol. 93, 1971, pp. 373–379.

[3]Andersen, P.S., Kays, W.M., and Moffat, R.J., "Experimental Results for the Transpired Turbulent Boundary Layer in an Adverse Pressure Gradient," *Journal of Fluid Mechanics,* Vol. 69, 1975, pp. 353–375.

[4]Kline, S.J., Cantwell, B.J., and Lilley, G.M. (eds.), *Proceedings of the 1980–81 AFOSR-HTTM-Stanford Conf. on Complex Turbulent Flows,* Dept. of Mechanical Engineering, Stanford Univ., Stanford, CA, 1980.

[5]Moin, P., "Numerical Simulation of Wall-bounded Turbulent Shear Flows," *Proceedings of the Eighth International Conference on Numerical Methods in Fluid Dynamics,* Springer-Verlag, New York, 1982.

[6]Piomelli, U., Ferziger, J.H., and Moin, P., "Models for Large Eddy Simulations of Turbulent Channel Flows including Transpiration," Dept. of Mechanical Engineering, Stanford Univ., Stanford, CA, Rept. TF-32, 1988.

[7]Bardina, J., Ferziger, J.H., and Reynolds, W.C., "Improved Subgrid Scale Models for Large Eddy Simulation," AIAA Paper 80-1357, July, 1980.

[8]Smagorinsky, J., "General Circulation Experiments with the Primitive Equations, I: The Basic Experiment," *Monthly Weather Review,* Vol. 91, 1963, pp. 99–164.

[9]Moin, P., Reynolds, W.C., and Ferziger, J.H., "Large Eddy Simulation of Incompressible Turbulent Channel Flow," Dept. of Mechanical Engineering, Stanford Univ., Stanford, CA, Rept. TF-12, 1978.

[10]Rajagopalan, S., and Antonia, R.A., "Some Properties of the Large Structure in a Fully Developed Turbulent Duct Flow," *Physics of Fluids,* Vol. 22, No. 4, 1979, pp. 614–622.